46th AIAA Aerospace Sciences Meeting and Exhibit, 7-10 January 2008, Reno, Nevada

Numerical Study of stall delay on humpback whale flippers

Hugo T. C. Pedro* and Marcelo H. Kobayashi
University of Hawaii, Holmes Hall 302, Honolulu, 96822, USA
Tel. (808) 956 8147 / email: hpedro@hawaii.edu

The low Reynolds numbers ($< 5 \times 10^5$) flows over wings have some unique features specially concerning separation. A comprehensive knowledge about this flight regime is extremely important for the autonomous aircrafts (UAV), since a large percentage of these vehicles operated in this regime.

In this report we simulate numerically the wind-tunnel experiments for two different wings inspired in the humpback whale flipper. One of the flippers displays a scalloped leading edge whereas the other one has a smooth leading edge. The experimental study revealed a significant increase in the aerodynamic performance for the scalloped flipper close to the separation. The detailed numerical solution allows for the complete characterization of the flow for both flippers.

The simulated Reynolds is (5×10^5) which allowed for the visualization of some of the low Reynolds effects. The comparison between the two geometries gives some indications about how to improve the aerodynamic performance of UAV's wings.

I. Introduction

The interest in small unmanned aerial vehicles (UAV's) has increased greatly in the past decade. The size of such vehicles and the velocity at which they operate results in low Reynolds (Re) number flight regime, in the $15000 - 500000$ range. The high Re aerodynamics is well established, however the same can not be said for the low Re regime. In this range the wing's aerodynamic performance can deteriorate rapidly as the Re number decreases.[1] To simply scale the vehicle to a smaller size is not the solution. Further research in this range of Re numbers is necessary.

Recently was reported[2] that the humpback whale flipper is optimized to prevent stall and to improve aerodynamic performance. These features allow these animals to be extremely mobile with great turning ability which is necessary to catch prey. This observation together with the fact that the Reynolds number for the humpback whale falls in the aforementioned low Re range propelled the experimental study the humpback whale flipper. The flippers for this species display a very characteristic scalloped leading edge, whereas the flippers of other species less maneuverable are much smoother.[3] The experiments compared a flipper with tubercles with a smooth flipper. The researchers reported an improvement in the aerodynamic performance as well an increase in the angle of attack at which the flipper stalls. However no flow visualization was performed, therefore the reasons why the scalloped flipper performs better were not uncovered.

In this work we performed the numerical simulation of the setup used for the experimental study. The unsteady turbulent flow field for the scalloped flipper and for the smooth flipper was accurately determined which produced detailed information necessary to fully understand the mechanism behind the reported improvement.

Our goal with this work is to increase the knowledge about these lower Re number flows which will be useful for the design of more efficient UAV's wings.

*This research was funded by the UH/MHPCC Engagement Grant.

II. Simulation Method

The flow around the flipper was modeled as incompressible at a Re number, based on the mean flipper chord, of 5×10^5. The numerical simulations were preformed with the commercial software package Fluent. This is a parallelized finite volume based code with several turbulence models implemented.

A. Governing Equations

The turbulent flow was solved using the DES (Detached Eddy Simulation) formulation. This formulation uses LES (Large Eddy Simulation) to solve the flow outside the boundary layer together with a Reynolds Averaged Navier-Stokes (RANS) to solve the boundary layer. Presently this is the best method we have available to solve turbulent flows since it provides good results at affordable computational costs. More accurate formulations, such as full LES and Direct Numerical Simulation (DNS) are expected to remain too costly in the next decades[4] for problems like the one we report here. Recently several successful simulations using DES were reported[5,6,7] that show the validity of this formulation. The DES model can be used with several RANS model, however Fluent only allows to use the one-equation RANS turbulence model Spalart-Allmaras. This is the natural choice, since, in fact the original DES model was based on the Spalart-Allmaras model.

Another affordable turbulence model could be the unsteady RANS, however this model was ruled out of consideration since it is inadequate to capture flows characterized by massive separation as we expect to find for the high angles of attack.[7]

B. Numerical Procedure

The numerical simulation used the segregated SIMPLE solver with a second order accurate spatial discretization. The time integration is performed with an implicit second order scheme.

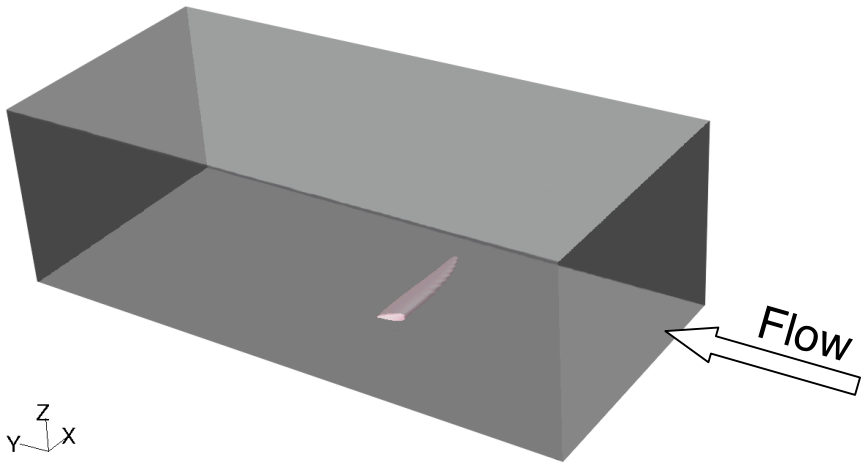

Figure 1. Problem geometry

C. Grid and Boundary Conditions

The simulations model the flipper and the wind tunnel test-section walls. The geometry modeled is shown in figure 1. The dimensions match the experimental setup with a tunnel's cross-section of 1.37×0.97 m and a tunnel's length of 3 m.

Both flippers are 56.25 cm long and have a projected plan-form area of 715 cm^2, which yields a mean chord of 12.7 cm. Reynolds number for the experiments was in the range 5.0×10^5 - 5.2×10^5. To maintain this value in our numerical simulation the velocity at the inflow boundary is 60 ms^{-1}, which corresponds to a Mach number of 0.18.

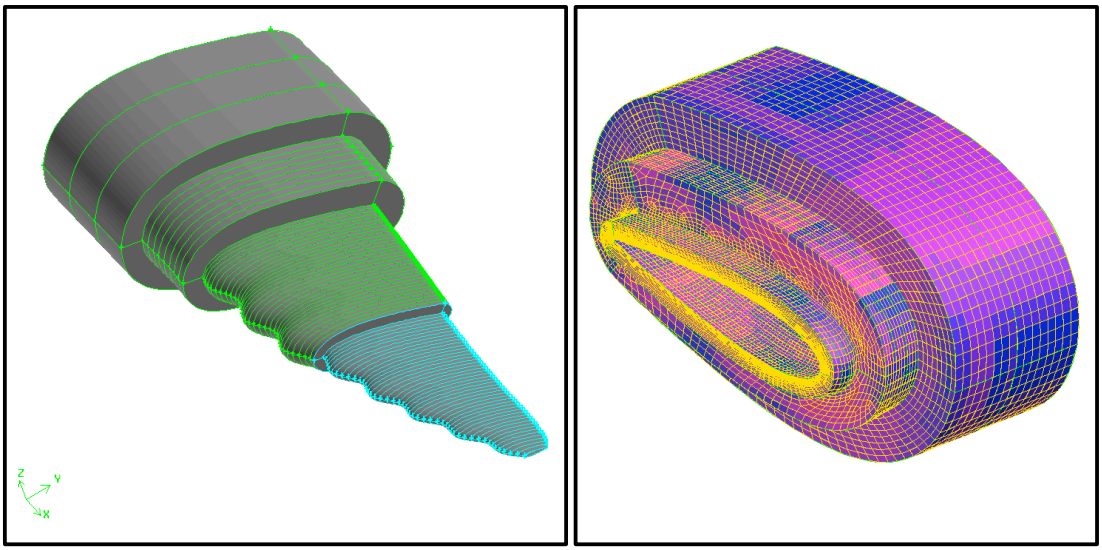

Figure 2. Geometry in the vicinity of the flipper, and close-up of the mesh

The mesh generation was done using the software package Gambit. This task proved to be very challenging specially for the scalloped flipper due to the complicated surface geometry. The mesh generation for the geometry showed in figure 1 using an unstructured mesh with tetrahedral elements proved to be cumbersome. Moreover it was very ineffective to control the element density close to the flipper. Therefore we choose to break our computational domain into smaller volumes as shown in figure 2. This option gave us total control over the mesh density. Besides this strategy allowed to mesh the domain using only hexahedral elements which increases the performance of the finite volume numerical method. An example of the mesh close to the flipper surface is depicted in Figure 2.

The number of elements in the blocks that enclose the flipper was set such that the value of y^+ is in the range 30 - 100 as recommended for the Spalart-Allmaras model. The mesh is progressively coarsened as the distance from the flipper increases. The meshes generated have about 2.6 millions elements. A rigorous grid dependence study was prevented by the large computational requirements of the unsteady simulation.

No-slip conditions were applied on the flipper and slip conditions on the wind tunnel walls, to avoid grid clustering close to this walls. The inflow boundary was placed 0.75 cm upstream of the flipper leading edge. The inlet velocity is normal to the inflow boundary for every angle of attack, which means that to simulate the exact experimental setup each angle of attack simulated is a different geometry and therefore a new mesh.

D. Simulation Start-up and Running

A steady RANS calculation was used as the starting point for the unsteady calculations. The steady RANS simulation allowed the flow field to develop quickly across the computational domain. The calculation was carried on until three or four orders of magnitude of convergence were obtained. This flow field was then

used as the initial condition for the time-dependent solution. The time step was set using the guidelines presented in[8] which yielded a time step of 0.0001 sec.

The duration of the simulation was determined beforehand by estimating the mean flow residence time in the solution domain ($L/U = 0.049$, where $L = 3$ m is the characteristic length of the solution domain and $U = 60$ m/s is a characteristic mean flow velocity). The simulation was run for 0.25 sec, which corresponds to 5 mean flow residence times. Hence, 2500 time steps were computed for each unsteady run. Generally speaking, the solution needs one to two mean flow residence times to attain statistical steadiness. The initial 1000 time-steps were not taken into account when time-averaged values where calculated.

The calculations were done on the MHPCC Tempest IBM P4 cluster using 32 CPU's. A full run required approximately 24 hours of wall-clock time.

III. Results and Discussion

In this section we present the comparison between the numerical results and the experiments. The numerical runs produced a huge amount of data that was processed to uncover the detailed flow dynamics. The results clearly show the differences between the two flipper geometries, besides it allows to fully characterize the separation mechanism.

A. Comparison With Experiment

As mentioned above the two flipper geometries were tested at a low speed wind tunnel. The reference[2] reports the experimental results both for C_L and C_D, which we use to compare against our results.

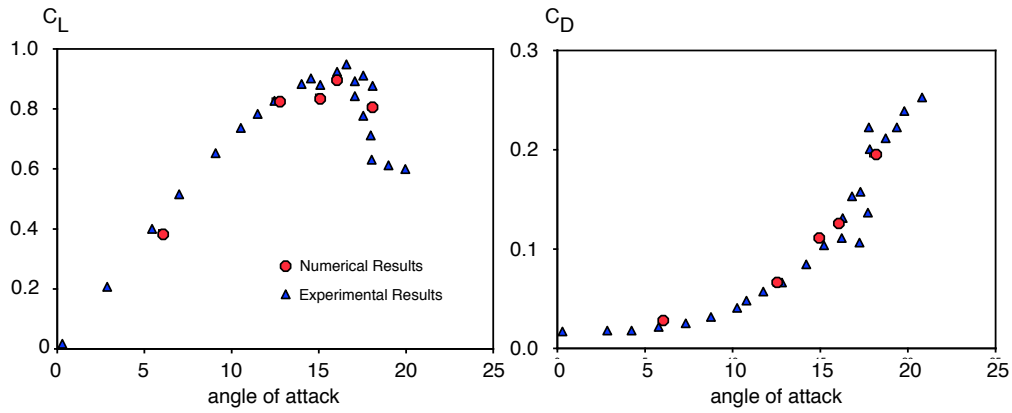

Figure 3. Force coefficients C_L and C_D as a function of the angle of attack for the scalloped flipper. Comparison between experimental and numerical results

Figure 3 depicts the results for the scalloped flipper. The numeric simulations were concentrated in the range of 12 - 18 angle of attack since the experiments determined this as the range were the different geometries showed the most noticeable differences. Only one run ($\alpha = 6^o$) was performed outside this range of values.

The numerical values shown in figures 3 and 4 are the average values for the statistically steady solution. They show a very good agreement with their experimental counterpart. The good agreement for C_L was expected since it's mainly due to the pressure imbalance between the upper and the lower sides of the flipper. Usually the pressure field is not problematic to predict accurately. However when separation occurs the results might suffer considerably. The good agreement even for $\alpha = 18^o$, for which the flow was clearly separated, shows the good quality of our results.

The C_D values for turbulent flows many times show a poor agreement with experimental values since a large percentage of this value is caused by skin friction, which is proportional to the velocity gradient at the surface. By using the RANS close to the wall we actually assume a log law for the velocity at the surface, this is often disadvantageous when one wants to determine an accurate values for C_D, however the values

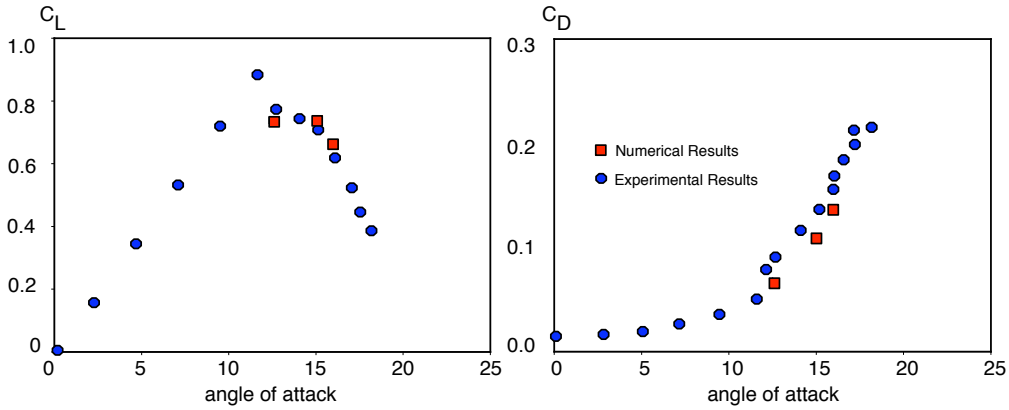

Figure 4. Force coefficients C_L and C_D as a function of the angle of attack for the smooth flipper. Comparison between experimental and numerical results

shown here display a very good agreement with the experiments. This is due to the fact that at these high angles of attack C_D is dominated by the form drag caused by the flow separation.

For the smooth flipper the results also show good agreement with the tunnel testes, however not as good as the ones for the scalloped flipper. The numerical C_D is lower than the experimental values. This dependence on the geometry is observed frequently: when a geometry displays strong features that determine the separation the numerical results are often better when compared to a similar smoother geometry that lacks those geometric features.

In spite of this small discrepancy, the forces show a good agreement with the experiments.

B. Detailed Simulation Results

In this section we analyze the flow dynamics in detail for both geometries. Our goal is to understand how separation occurs, and to uncover the reason for the better performance of the scalloped flipper. The experiments revealed that the angle of attack for which the difference in terms of the forces is most noticeable is $\alpha = 15^o$ therefore we focussed our analysis on this angle of attack.

1. Contours of pressure and vorticity

One of the most important questions we want to clarify is wether or not the leading-edge tubercles in the scalloped flipper work as vortex generators. The basic principle of those devices is to generate stream-wise vortices, hence the analysis of vorticity at the flipper surface is of prime importance. In figure 5 it is depicted an isosurface of vorticity magnitude. The value is the same for both figures (a) and (b).

The figure shows that at the root and the tip both flippers produce similar vortical structures. Has one could expect the most noticeable stream-wise vortex at these locations is the tip vortex. The outboard 1/5 as well as the root of both wings are covered by large vortical structures, which seem somewhat chaotic. Indeed, as we shall demonstrate ahead in these regions the flow is separated giving rise to chaotic flow motion.

In the flipper midsection that similarity completely vanishes. Instead, we observe that the scalloped flipper displays large stream-wise vortices aligned with the tubercles. On the other hand the smooth flipper shows no such structures. In figure 6 we can assess more clearly the difference in the vorticity field. The high values of vorticity over the midsection of the scalloped flipper locate the center of rotation of the stream-wise vortices. These eddies re-energize the boundary layer by carrying high momentum flow close to the wall. In figure 7 we can observe how effectively the vortices energize the near wall flow. This figure displays the isosurface for the same value of $|V|^2$ in the two flipper geometries. This quantity is proportional to the momentum carried by the fluid.

The improvement in the outboard section of the flipper is clear. The flow over the scalloped flipper possesses much more momentum in this region, which delays the separation.

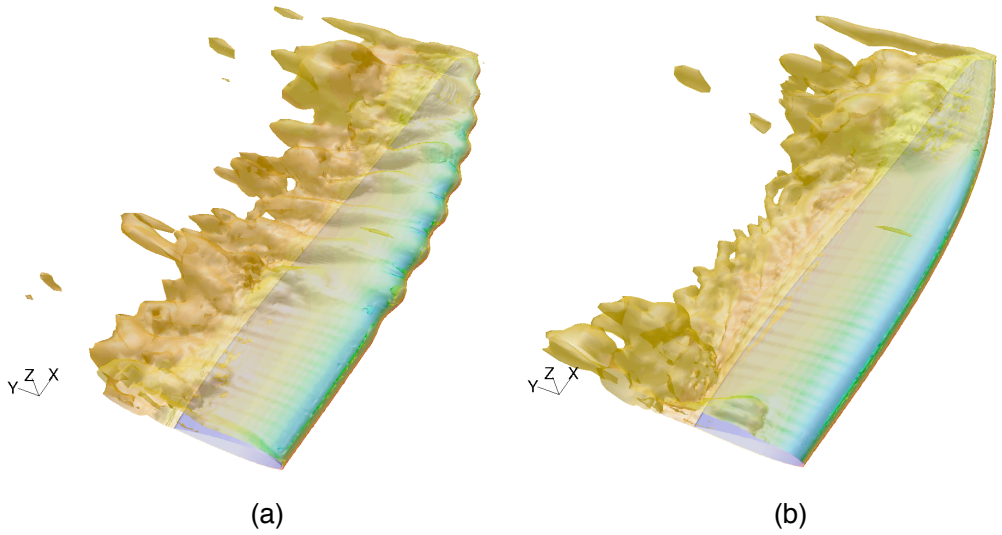

Figure 5. Instantaneous vorticity magnitude isosurface colored by pressure for $\alpha = 15^o$. (a) Scalloped flipper, (b) smooth flipper.

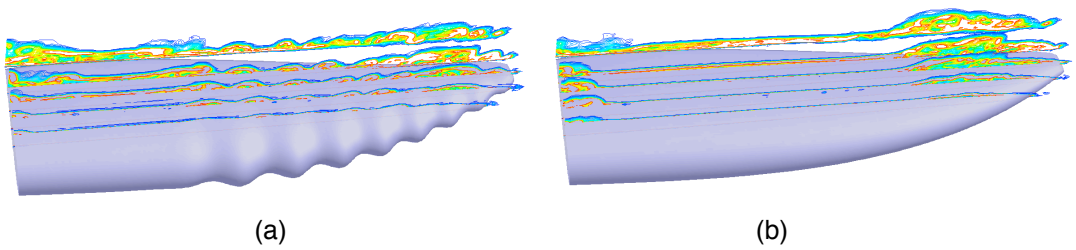

Figure 6. Instantaneous vorticity magnitude slices in the chord-wise direction for $\alpha = 15^o$.(a) Scalloped flipper, (b) smooth flipper. The color scale is the same for both figures.

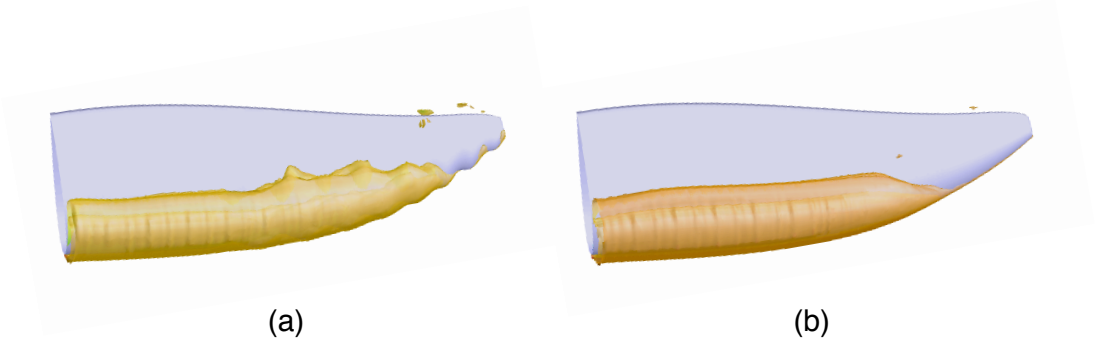

Figure 7. Instantaneous $|V|^2$ isosurface colored by pressure for $\alpha = 15^o$.(a) Scalloped flipper, (b) smooth flipper.

2. Separation

As mentioned in the introduction the problem here reported is in the threshold of low Reynolds numbers problems. However due to the large span-wise variations of the flipper's chord we can identify two different regions in terms of the Reynolds number. The average Reynolds number for the outboard third of the flipper is clearly a low Reynolds number (< 200000), whereas the inboard section's Re falls in the category of high Reynolds numbers (> 500000).

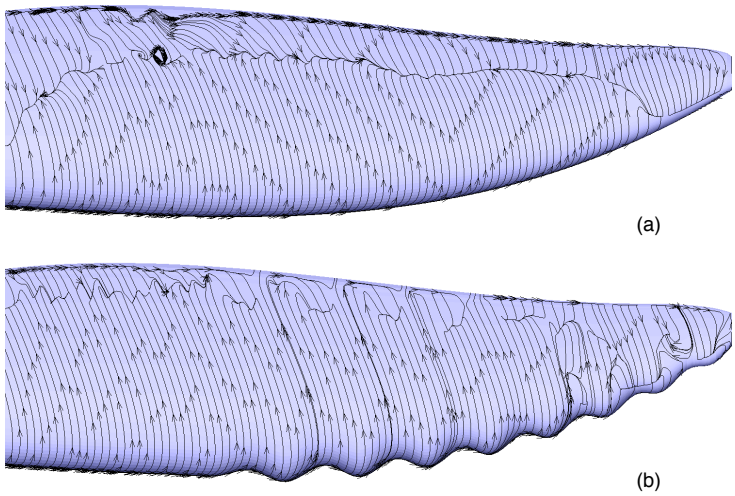

Figure 8. Averaged shear stress streak-lines for $\alpha = 12.5^o$.(a) Scalloped flipper, (b) smooth flipper.

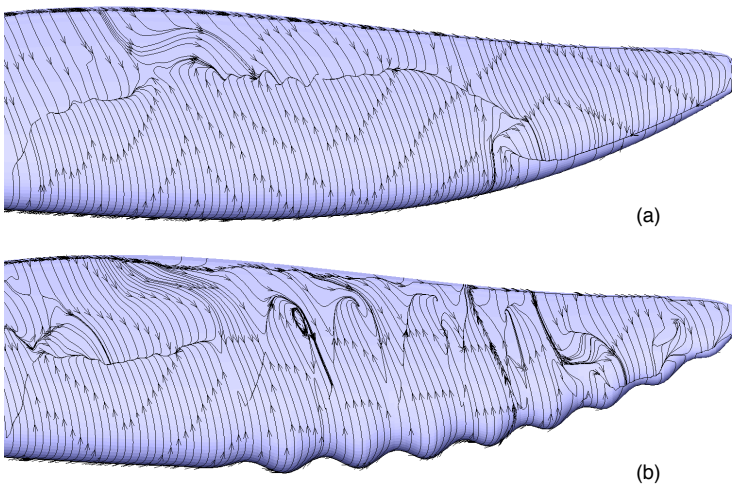

Figure 9. Averaged shear stress streak-lines for $\alpha = 15^o$.(a) Scalloped flipper, (b) smooth flipper.

The study of separation is done by investigating the shear stress at the flipper's surface. In figure 8 and 9 the averaged shear stress streak-lines at the flipper surface are displayed. When the streak-lines point in the flow direction the flow is attached whereas the reversed indicates flow separation and the line to which the streak-lines are attracted represents the separation line.

These figures clearly show that the two aforementioned regions display completely different types of

separation. In the outboard section the flow separates in the leading edge whereas in the inboard section we observe a trailing edge type of flow separation. This characteristic is common to both flipper geometries. This type of separation can be very damaging for the flipper performance since the separated region can grow very fast in the root direction. Indeed, the smooth flipper displays that behavior. The increase of the angle of attack from 12.5 to 15 degrees propagates the separation region rapidly towards the flipper's root. As we saw previously in the aerodynamic forces plots this damages the aerodynamic performance greatly by decreasing C_L sharply and increasing C_D. As for the scalloped flipper, we observe that the separated region for $\alpha = 12.5^o$ is comparable to that of the smooth flipper, however in this case the change in the angle of attack did not increase the separation so dramatically. This behavior resembles another passive separation control that can be found in real aircrafts: the wing fence. These devices create a physical barrier to the span-wise motion which prevents the separation growth from the tip to the root of the wing.

These figures also demonstrate that the scalloped flipper resists to separation more efficiently than the smooth flipper in the high Reynolds region, as well. Once again the explanation is based on the presence of the stream-wise vortices that energize the trailing portion of the flipper delaying separation.

IV. Conclusion

The most important findings reported here can be summarized in the following manner:

(i) The low Reynolds number influences the type of separation observed in the flipper. The outboard section, dominated by lower Reynolds regime displays a leading edge type of separation; the inboard section display trailing edge separation.

(ii) The higher aerodynamic performance for the scalloped flipper is due to the presence of stream-wise vortices originated by the tubercles. The reason why it improves the aerodynamics is twofold. In first place the vortices carry momentum to the boundary layer delaying the trailing-edge separation, secondly these vortices confine the leading edge separation to the tip region.

(iii) The DES turbulence model was successfully used to determined the flipper aerodynamics in the range of low Reynolds numbers.

References

[1]Mueller1, T. J. and DeLaurie, J. D., "Aerodynamics of small vehicles," *Annu. Rev. Fluid Mech*, Vol. 35, 2003, pp. 89 – 111.

[2]D. S. Miklosovic, M. M. Murray, L. E. H. and Fish, F. E., "Leading-edge tubercles delay stall on humpback whale (Megaptera novaeangliae) flippers," *Physics of Fluids*, Vol. 16, 2004, pp. 39 – 42.

[3]Becky L. Woodward, J. P. W. and Fish, F. E., "Morphological Specializations of Baleen Whales Associated With Hydrodynamic Performance and Ecological Niche," *Journal of morphology*, Vol. 267, 2006, pp. 1284 – 1294.

[4]Spalart, P., "Strategies for turbulence modelling and simulations," *International Journal of Heat and Fluid Flow*, Vol. 21, 2000, pp. 252 – 263.

[5]L. S. Hedges, A. T. and Spalart, P., "Detached-Eddy Simulations Over a Simplified Landing Gear," *Journal of Fluids Engineering*, Vol. 124, 2002, pp. 413 – 423.

[6]Scott Morton, James Forsythe, A. M. and Hajek, D., "Detached-Eddy Simulations and Reynolds-Averaged Navier-Stokes Simulations of Delta Wing Vortical Flowfields," *Journal of Fluids Engineering*, Vol. 124, 2002, pp. 924 – 932.

[7]Andrei Travin, Michael Shur, M. S. and Spalart, P., "Detached-Eddy Simulations Past a Circular Cylinder," *Flow, Turbulence and Combustion*, Vol. 63, 2000, pp. 293 – 313.

[8]Spalart, P., "Young-Person's Guide to Detached-Eddy Simulation Grids," *NASA/CR-2001-211032*, 2001.